J Mater Sci
DOI 10.1007/s10853-015-9334-0

50TH ANNIVERSARY

Quantitative correlation of interfacial contamination and antiphase domain boundary density in GaAs on Si(100)

C. S. C. Barrett[1] · A. G. Lind[1] · X. Bao[2] · Z. Ye[2] · K. Y. Ban[2] · P. Martin[2] · E. Sanchez[2] · Y. Xin[3] · K. S. Jones[1]

Received: 31 May 2015 / Accepted: 5 August 2015

Abstract The role of interfacial contamination on antiphase domain boundary (APB) formation in GaAs grown epitaxially on Si(100) by metal-organic chemical vapor deposition was investigated. The pre-growth cleaning of the Si substrate was varied to affect the relative amount of residual surface contamination across the wafer. APB density in the as-grown GaAs film was examined with the aid of a selective APB etchant. The interfacial oxygen and carbon concentrations were determined using secondary ion mass spectrometry. It was found that the APB density increased significantly from 0.14 to 3.2 μm^{-1} between the center and the edge of the wafer. Over this distance, the integrated carbon concentration at the GaAs/Si interface increased by an order of magnitude and the integrated oxygen concentration, although two orders of magnitude lower than carbon, also increased by a factor of six. Analysis of the GaAs/Si interface with high-resolution transmission electron microscopy and high-angle annular dark field scanning transmission electron microscopy showed a direct association of APBs with amorphous interfacial particles. The particles are likely carbon-based, possibly SiC, and thus residual carbon contamination is believed to be the primary contributor to increased APB formation.

✉ C. S. C. Barrett
cscbarrett@ufl.edu

[1] Department of Materials Science and Engineering, University of Florida, Gainesville, FL 32611, USA

[2] Applied Materials, 974 East Arques Avenue, Sunnyvale, CA 94085, USA

[3] National High Magnetic Field Laboratory, Florida State University, Tallahassee, FL 32310, USA

Introduction

As electronic device scaling approaches the sub-10 nm regime, there is growing interest in the use of alternative channel materials in metal-oxide-semiconductor field effect transistors (MOSFETs). These new materials should allow for further scaling with reduced power consumption compared to conventional Si-based devices without compromising transistor quality or electrical performance. III–V compound semiconductors such as InGaAs or InAs are good candidates for future n-channel MOSFET devices because of their excellent electron transport properties and potential for reduced contact resistance [1]. However, in order to realize large-scale production of III–V devices, fabrication must continue to be performed on Si wafers. Obtaining a high-quality III–V layer on Si is a significant barrier to the successful implementation of III–V channel materials.

III–V epitaxial layers grown directly on Si substrates are typically plagued by high densities of defects that degrade electrical performance. The lattice mismatch between the III–V film and Si induces a large number of threading dislocations that propagate through the layer. For an InAs-on-Si film, this mismatch is about 12 % (lattice constant of 6.06 vs. 5.43 Å). There are already well-developed strategies to reduce the density of threading dislocations in III-V films, including aspect ratio trapping (ART) [2, 3] and the use of buffer layers [4–6]. GaAs is well-suited as a buffer layer for InGaAs and InAs grown on Si due to its intermediate lattice constant (5.65 Å) and relatively large bandgap for electrical isolation.

The nature of growing a polar epitaxial film on a non-polar substrate can also lead to the formation of antiphase domains (APDs) [7]. These domains are regions in the film that have a reversed polarity compared to the bulk crystal

Published online: 13 August 2015

[8]. APDs in GaAs have been studied for several decades [9–14]. They were first predicted to form in III–V compounds by Holt in 1969 [15] and then were experimentally observed in epitaxial GaAs films by Morizane in 1977 [9]. It is now well-understood that a single-step present on the substrate surface prior to film growth can disrupt the epitaxial crystal ordering and cause the nucleation of an antiphase domain boundary (APB) [16]. An APB is a planar defect defined by having similar atoms in a III–V film bonded across the APB, e.g., Ga–Ga and As–As in GaAs. Consequently, APBs have very large associated energies [17] and have detrimental effects on device performance as they can propagate entirely through a layer. In theory, APBs can be eliminated by having a double-stepped substrate surface. However, this typically requires a high temperature annealing treatment near 1000 °C prior to growth to induce a reconstruction of the (100) Si surface [18–20] or the use of off-cut Si wafers [21]. These methods are not compatible with conventional CMOS processing which requires reduced thermal budgets and nominally planar substrates [22]. Thus, self-annihilation of APBs through propagation along higher-index planes [23–25], e.g., {111}, remains the only practical way of suppressing APBs within the III-V layer under the above stated restrictions. Such self-annihilation during growth has been observed in a GaAs-on-Si system, leading to a decrease in APB density with increasing film thickness [12].

Contamination is a critical issue in semiconductor growth and processing. Impurities present on substrate surfaces prior to epitaxial layer growth can disrupt the growth kinetics of the layer and lead to higher densities of defects, e.g., stacking faults and dislocations [7, 26–30]. These impurities are commonly oxygen or carbon based. While increased interfacial contamination is associated with lower overall crystal quality of the epitaxial layer, the effect on APB formation is less clear. Higher densities of APBs will be more difficult to completely annihilate within a film of a given thickness. It has been speculated that interfacial contamination can contribute to APB formation [7, 28] but never systematically studied. The goal of this work is to provide greater insight on the relationship between interfacial contamination and the formation of APBs in an epitaxial GaAs film grown on Si(100) by metal-organic chemical vapor deposition (MOCVD) without the use of a high temperature pre-growth anneal near 1000 °C or wafer off-cut typically used to suppress APB nucleation.

Materials and methods

A 300 mm (100) oriented Si wafer with no intentional off-cut was utilized as the substrate in this study. The substrate was cleaned prior to growth using a Siconi^{TM} etch process [31]. This method involves a dry remote fluorinated plasma that selectively reacts with and removes native oxide. The cleaning process was varied across the wafer in order to affect the relative amount of residual surface contamination from the center to edge. By modulating the residual contamination on a single wafer, identical growth conditions are ensured for specimens taken from different areas of the wafer. The substrate was then baked at a moderate temperature (<1000 °C) to help promote the formation of double-steps.

A nominally 450 nm thick epitaxial GaAs film was subsequently grown on the Si substrate with an Applied Materials III–V MOCVD system. The precursors for Ga and As were trimethylgallium (TMGa) and tertiarybutylarsine (TBAs), respectively. GaAs growth was carried out using the well-established two-step growth method for III–V epitaxy at typical reduced pressure ambient to aid in nucleation and improve crystal quality [32, 33]. In this process, a low temperature step is first used to nucleate the film followed by bulk growth at a higher temperature in the conventional GaAs homoepitaxy range.

After growth, specimens were taken from the center to edge of the wafer in sequential order. The APB density in the as-grown GaAs film for each specimen was determined using scanning electron microscopy (SEM) with the aid of a HF(49 %):HNO_3(69 %):H_2O (10:1:3 by volume) etchant to improve contrast of APBs. The HF/HNO_3 solution has been demonstrated to be selective for APBs in GaAs [11–13]. The samples were dipped in the solution at room temperature for a short time (<10 s). Cross-sectional TEM (XTEM) through an etch feature was used to verify that the etchant was preferentially etching the APBs. SEM images in plan view were collected in various areas of the sample. The line length of APBs was determined using ImageJ software [34]. The APB density is defined as the line length of APBs per unit area, giving units of μm^{-1}.

The oxygen and carbon concentration depth profiles in the GaAs films were obtained using secondary ion mass spectrometry (SIMS). Samples were sputtered using Cs^+ ions. The depth resolution was $\sim$1 nm. The integrated interfacial oxygen and carbon doses were determined from the corresponding peaks at the location of the GaAs/Si interface.

Samples for XTEM were prepared using a focused ion beam (FIB) system. HRTEM imaging of the GaAs layers and GaAs/Si interface was performed using a JEOL 2010F instrument. Annular bright field scanning transmission electron microscopy (ABF-STEM) and high-angle annular dark field scanning transmission electron microscopy (HAADF-STEM) imaging were carried out using a probe aberration-corrected JEM-ARM200cF instrument with the STEM resolution of 0.78 Å. HAADF-STEM images were acquired with a probe convergence semi-angle of 11 mrad and collection angles of 76-174.6 mrad.

Results and discussion

Representative SEM images of sample surfaces after applying the HF/HNO_3 stain are shown in Fig. 1a–c for specimens from the center, 8 cm from the center, and the edge of the wafer, respectively. The increase in APB density is apparent and the behavior of APBs also changes. Domains in the specimen from the wafer center (Fig. 1a) are much more self-contained and demonstrate clear faceting along crystallographic planes. At a distance +8 cm from the center of the wafer (Fig. 1b), domains reach larger overall dimensions and the APBs begin to lose faceting behavior. Finally, at the edge of the wafer (Fig. 1c), APBs curve and extend for relatively long distances and it becomes difficult to distinguish isolated domains. Figure 2 shows the APB density measurements of samples taken in 2 cm increments from the center to the edge of the wafer. The APB density increases significantly from 0.14 ± 0.01 μm^{-1} at the center to 3.2 ± 0.3 μm^{-1} at the edge (>20× increase). The greatest rate of increase is in the middle region from +6 cm to +10 cm relative to the center of the wafer. GaAs film thickness was determined to range from 455 nm at the center to 445 nm at the edge using XTEM (not shown). This minimal thickness difference is unlikely to account for the observed change in APB density from any additional self-annihilation of APBs and also indicates that the growth process is fairly uniform. The significant increase in APB density suggests another factor is varying systematically from the center to the edge of the wafer, most likely from the pre-clean treatment.

The amount of oxygen and carbon contamination present at the GaAs/Si interface was investigated with SIMS. The interfacial oxygen and carbon concentration peaks are shown in Fig. 3a, b, respectively. Depth profiles were obtained for samples from the center, +6 cm from the center, +8 cm from the center, +10 cm from the center, and the edge of the wafer, corresponding to the two extremes of APB density and the transition region. The interfacial peak positions were normalized to the sample

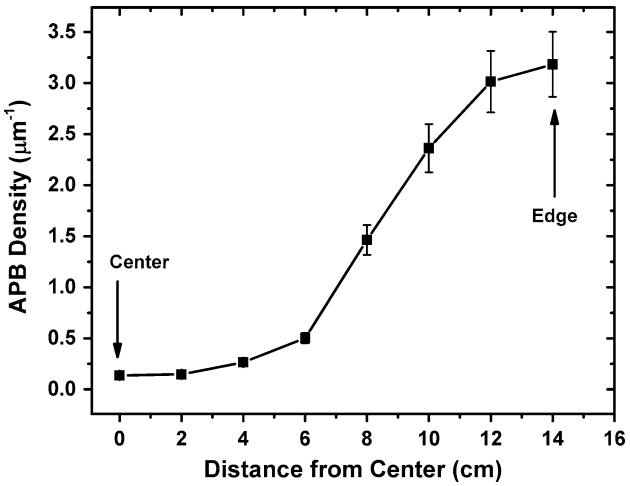

Fig. 2 APB density in the as-grown GaAs-on-Si film versus position on the wafer. Specimens were taken from the wafer in sequential order every 2 cm from the center to edge

layer thickness as determined by XTEM. There is a trend of increasing peak oxygen and carbon concentration from the center to the edge of the wafer. It is evident that the overall peak carbon concentration (Fig. 3b) is much greater than that of oxygen (Fig. 3a). A large contributor to the carbon depth profile is likely incorporation of the precursor reaction products; however, there is still a distinguishable interfacial peak as highlighted by the inset in Fig. 3b. This area is used to determine the interfacial carbon dose. The increase in oxygen and carbon concentration from the center to the edge of the wafer likely stems from the variation in the pre-clean treatment. An additional source of carbon contamination could be carbon desorbed from the MOCVD chamber walls during the pre-growth bake. Any such carbon species would be more likely to reach the edge of the wafer than the center.

Figure 4 plots the interfacial oxygen and carbon doses, as determined by integration of the interfacial peaks in the SIMS profiles, versus the corresponding location of each sample on the wafer. The oxygen dose increases from

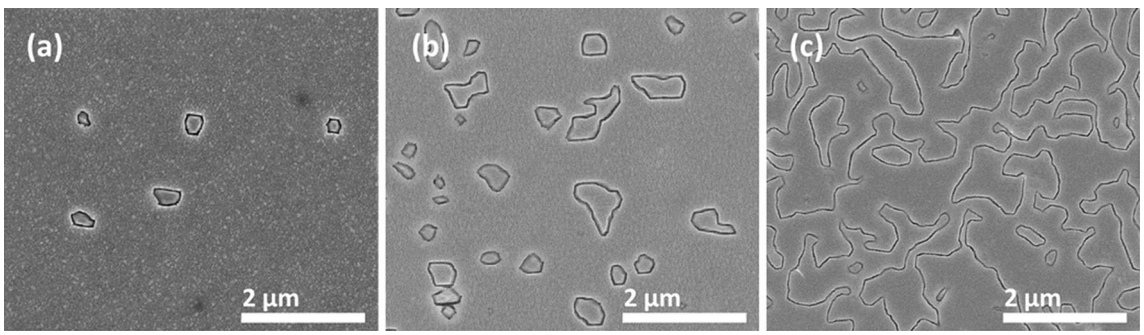

Fig. 1 Plan view SEM images of sample surfaces from the center (**a**), +8 cm from the center (**b**), and the edge (**c**) of the wafer after staining with HF/HNO_3 solution to selectively etch APBs. The APBs are clearly delineated after etching with dark contrast

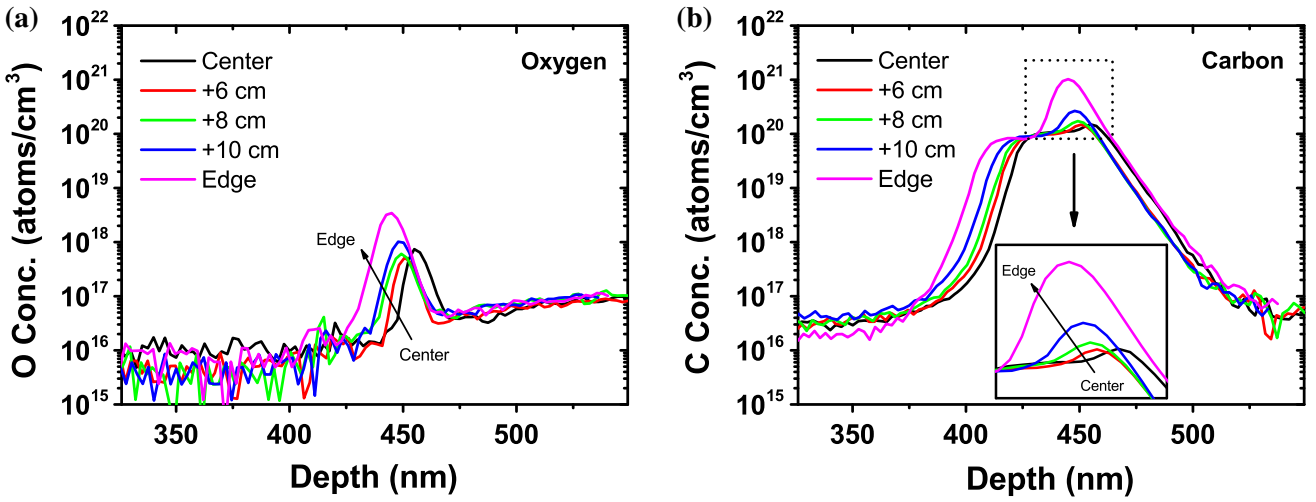

Fig. 3 Concentration depth profiles obtained by SIMS for oxygen (**a**) and carbon (**b**) for selected samples. Peaks at the GaAs/Si interface are shown. Peak positions are normalized to film thickness as observed in XTEM. *Inset* in (**b**) shows peak region used for calculation of interfacial carbon dose (Color figure online)

7.3×10^{11} atoms/cm^2 at the center to 4.0×10^{12} atoms/cm^2 at the edge, while the carbon dose increases from 1.9×10^{14} atoms/cm^2 at the center to 1.7×10^{15} atoms/cm^2 at the edge. Note that the oxygen dose is slightly greater at the center than at +6 and +8 cm from the center, corresponding to greater peak concentration in Fig. 3a. Both oxygen and carbon dose follow the same approximate trend across the wafer which corresponds well with the change in APB density (Fig. 2). However, the significant difference by over two orders of magnitude between oxygen and carbon dose indicates it is more likely that carbon-based impurities are causing the observed effects on APB density.

Figure 5 shows the relationship between the measured APB density and integrated interfacial carbon dose for specimens from corresponding positions of the wafer. The plot follows a logarithmic trend before the APB density begins to plateau. This quantitative correlation between interfacial carbon contamination and APB density suggests that carbon-based impurities present on the Si substrate prior to GaAs growth are contributing to APB formation in the GaAs layer. There is also an indication of a threshold effect from residual carbon contamination, i.e., APB density increases significantly after $\sim 2 \times 10^{14}$ atoms/cm^2 of interfacial carbon dose. Thus, it is important to reduce interfacial contamination to minimize APB density in the film and in turn minimize the layer thickness necessary to completely suppress APBs. It is possible that amorphous impurity particles disrupt atomic ordering in the growing

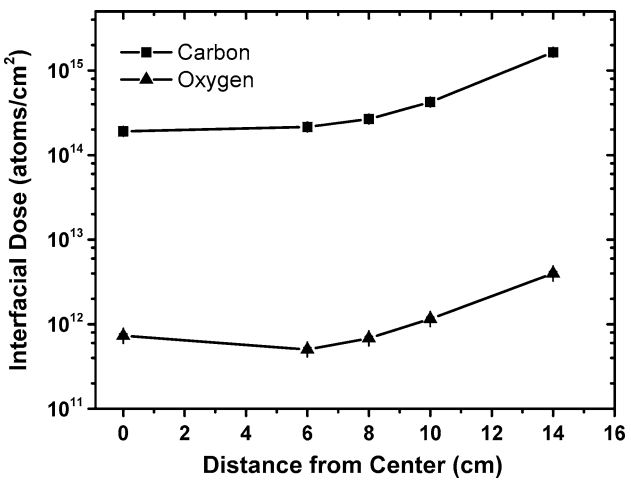

Fig. 4 Integrated oxygen and carbon doses at GaAs/Si interface versus position on wafer relative to the center for SIMS data of samples shown in Fig. 3a, b

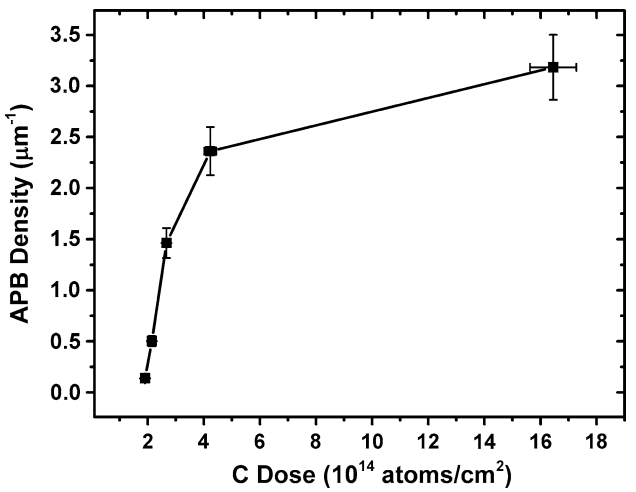

Fig. 5 APB density versus interfacial carbon dose for samples at similar wafer positions. APB density increases from 0.14 to 3.2 μm^{-1} over a 1.9×10^{14} to 1.7×10^{15} atoms/cm^2 range of carbon dose

film similar to single-steps, and thus give rise to a greater overall APB density versus samples with lower amounts of carbon contamination.

Examination of the GaAs/Si interface with HRTEM was conducted to investigate the physical relationship between residual interfacial impurities and APB formation. Figure 6a shows a region of the GaAs/Si interface in cross-section along the [011] zone axis in a specimen from the edge of the wafer, corresponding to higher amounts of oxygen and carbon contamination. The distribution of distinct particles along the interface is observed (indicated by arrows). Figure 6b is a higher magnification image of a particle in the same region of the specimen seen in Fig. 6a. The particle is amorphous and induces the formation of planar defects along {111} planes, e.g., micro twins or stacking faults. A group of micro twins or stacking faults is seen to be terminating ~15 nm away from the particle (marked by the arrow), indicating the presence of an APB that is also associated with the particle. The high energy and degree of lattice disorder of an APB makes it likely that defects such as stacking faults and micro twins will terminate at an APB, which agrees with experimental TEM observations [12, 28, 35].

Further investigation of the interfacial particles was carried out using ABF-STEM and HAADF-STEM imaging for the sample from the edge of the wafer. A region of the GaAs/Si interface is seen in ABF and HAADF in Fig. 7a, b, respectively. An amorphous particle (indicated by the arrow) is clearly observed at the interface in Fig. 7a. An APB appears to be emanating from the particle in Fig. 7b, as indicated by reversal of the Ga-As bond polarity ("dumbbells") across the indicated boundary. The variation in image intensity of the Ga and As atoms (atomic number difference of 3) shows As atoms on top of Ga atoms on the left of the line, and Ga atoms on top of As atoms on the right (Fig. 7b), demonstrating that this is an APB. The Fourier-filtered image of Fig. 7b using the 200 type spots is shown in Fig. 7c. The misordering of (200) planes by ~1/2 plane spacing across the APB can be seen. This misordering is characteristic of an APB due to the inversion of the GaAs crystal structure [36] and is consistent with experimental observations in a similar GaSb-on-Si system [35]. These observations present direct evidence for the nucleation of an APB by an amorphous interfacial particle, as has been previously speculated [7]. The APBs nucleated by particles would form in addition to those caused by single-steps and contribute to greater overall APB density in the film compared to samples with lower amounts of residual contamination.

The chemical identity of the particles is unclear, but further evidence can be gathered by calculating the expected distribution of particles along the GaAs/Si interface from the interfacial oxygen and carbon contamination doses and the observed particle size in TEM. The particles are assumed to be either amorphous SiO_2 or SiC. Dimensions of standard particle size are taken from Fig. 6b and the particles are assumed to be circular. Thus, the number of oxygen or carbon atoms per particle can be calculated. The oxygen and carbon interfacial doses for the edge sample were 4.0×10^{12} atoms/cm^2 and 1.7×10^{15} atoms/cm^2, respectively. By dividing the interfacial doses by the corresponding particle atomic densities, the expected areal density of oxygen or carbon particles can be determined. Finally, the areal density is multiplied by the thickness of the FIB-produced lamella of 50 nm to obtain an expected

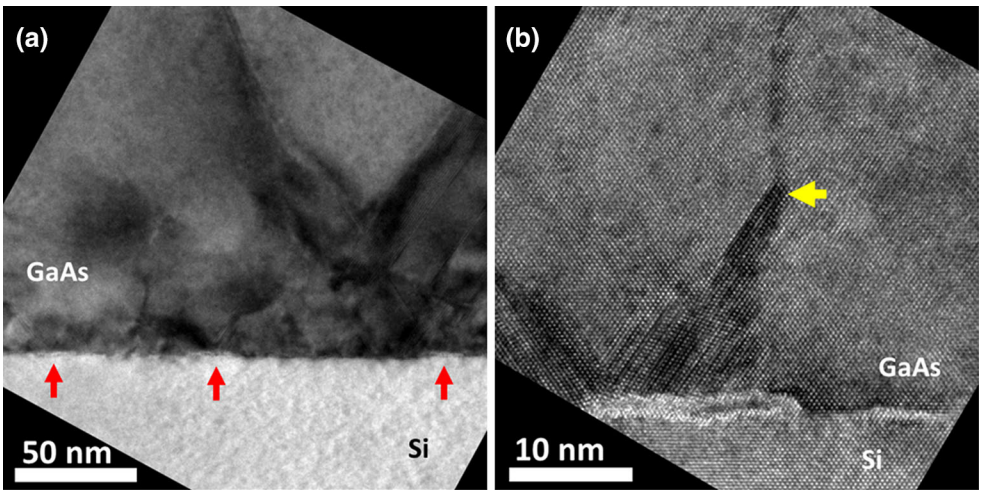

Fig. 6 Cross-sectional HRTEM images along the [011] zone axis of a sample from the edge of wafer (4.0×10^{12} atoms/cm^2 oxygen dose and 1.7×10^{15} atoms/cm^2 carbon dose). Locations of interfacial particles are marked by arrows in (**a**). A higher magnification of a particle seen in (**a**) is shown in (**b**) and an APB emanating from the particle and terminating a stacking fault or micro twin is marked by an *arrow*

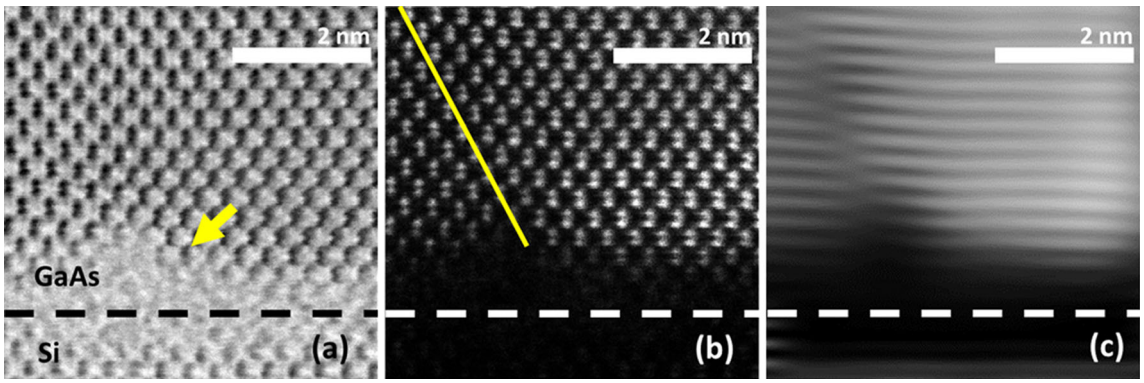

Fig. 7 Cross-sectional images of identical region of GaAs/Si interface along the [011] zone axis in ABF-STEM (**a**) and HAADF-STEM (**b**) for sample from the edge of the wafer. A Fourier-filtered image of (**b**) using the 200 spots is shown in (**c**). An amorphous particle is marked by the arrow in (**a**). An APB is observed emanating from particle in (**b**) and the offset of (200) planes at the APB is clearly visible in (**c**). Approximate position of GaAs/Si interface is indicated by *dashed line*

spacing of both SiO_2- and SiC-based particles that would be observed in XTEM. If the particles are oxygen-based SiO_2, the expected particle spacing is $\sim$16 μm. For carbon-based SiC particles, the expected spacing is $\sim$40 nm which is consistent with the particle spacing seen in Fig. 6a. Simply, carbon is the only impurity present in enough quantity to account for the presence of the particles. Thus, the interfacial particles associated with the formation of APBs and other planar defects are likely carbon-based, possibly SiC.

An alternative explanation for the association of APBs with amorphous particles is not a direct nucleation effect due to disruption of atomic ordering but the passivation of single-steps on the Si surface prior to GaAs growth by residual carbon contamination. APBs form at single-steps because of the rotation of the Si (2 × 1) dimers on the (100) surface step terraces [7] which in turn causes rotation of the epitaxial GaAs lattice. Thus, it may not be plausible for an APB to solely nucleate from a particle in the absence of a single surface step. Rather, residual carbon may be agglomerated at single-step sites to terminate dangling bonds and lower the overall free energy. Carbon has been observed to preferentially collect at step sites on (100) Si surfaces [37]. Single-step sites on the Si substrate with agglomerated carbon are then essentially passivated and are less likely to reconstruct to double-steps during the annealing process prior to GaAs growth. In turn, regions with higher amounts of carbon contamination will have a greater density of single-steps, and thus a greater APB density in the film. It is unclear whether this is effect would be significant enough to cause the observed variation in APB density and behavior. Further investigation of the Si substrate surface after the cleaning step but prior to GaAs growth is needed.

Thus, it appears the relative amount of residual surface contamination does have an effect on the formation of APBs in GaAs-on-Si. It is not explicitly determined whether the source of contamination causing the observed effects on APB formation is oxygen or carbon. However, the much greater amount of interfacial carbon versus interfacial oxygen along with TEM observations suggests carbon is the more likely source. Smaller self-contained domains and lower overall APB density, as observed in Fig. 1a, are advantageous for annihilation of APBs within the GaAs films due to the inherent tendency of APBs to kink to higher-index planes and self-annihilate with growth thickness [12, 23]. Reducing contamination and thus reducing the APB density should allow for complete suppression of APBs with minimized GaAs layer thickness. This is ideal for the use of GaAs as a buffer layer to integrate other III-V transistor channel materials on Si for future devices.

Conclusions

In conclusion, it was shown that there is a quantitative correlation between the APB density in a GaAs-on-Si film and the amount of interfacial contamination. The primary source of contamination affecting the formation of APBs is most likely carbon-based amorphous particles, e.g., SiC. For a range of interfacial carbon dose of 1.9×10^{14} atoms/cm^2 to 1.7×10^{15} atoms/cm^2, the APB density increased logarithmically from 0.14 to 3.2 μm^{-1}. TEM analysis of the GaAs/Si interface showed a direct association of APBs with amorphous particles. It is unclear if the APB is in fact being nucleated by the particle or if there is an indirect effect of carbon agglomeration at single-step sites. With either explanation, there is a clear contribution of residual contamination to additional formation of APBs. The significant increase of APB density after $\sim 2 \times 10^{14}$ atoms/cm^2 of interfacial carbon dose indicates there is a critical

threshold for reduction of surface contamination to minimize APB formation and in turn minimize epitaxial layer thickness. This result is important for the integration of GaAs and other III-Vs in future electronic devices without the use of typical strategies for the suppression of APB nucleation (i.e., the use off-cut wafers and high-temperature treatments) that are incompatible with conventional CMOS processing.

Acknowledgements This work is funded through a research grant by Applied Materials. The Major Analytical Instrumentation Center at the University of Florida is thanked for the use of the focused ion beam and transmission electron microscopy facilities. The TEM facility at Florida State University is funded and supported by the FSU Research Foundation, and the National High Magnetic Field Laboratory, supported by the National Science Foundation Cooperative Agreement DMR-1157490, the State of Florida.

Compliance with ethical standards

Conflict of interest Authors C. S. C. Barrett, A. G. Lind, and K. S. Jones have received research grants from Applied Materials, Inc., and K. S. Jones has consulted for Applied Materials.

References

1. Del Alamo JA (2011) Nanometre-scale electronics with III–V compound semiconductors. Nature 479:317–323. doi:10.1038/nature10677
2. Li JZ, Bai J, Park J-S et al (2007) Defect reduction of GaAs epitaxy on Si (001) using selective aspect ratio trapping. Appl Phys Lett 91:021114. doi:10.1063/1.2756165
3. Cipro R, Baron T, Martin M et al (2014) Low defect InGaAs quantum well selectively grown by metal organic chemical vapor deposition on Si(100) 300 mm wafers for next generation non planar devices. Appl Phys Lett 104:262103. doi:10.1063/1.4886404
4. Choi D, Harris JS, Kim E et al (2009) High-quality III–V semiconductor MBE growth on Ge/Si virtual substrates for metal-oxide-semiconductor device fabrication. J Cryst Growth 311:1962–1971. doi:10.1016/j.jcrysgro.2008.09.138
5. Cantoro M, Merckling C, Jiang S et al (2013) Heteroepitaxy of III–V compound semiconductors on silicon for logic applications: selective area epitaxy in shallow trench isolation structures vs. direct epitaxy mediated by strain relaxed buffers. ECS Trans 50:349–355. doi:10.1149/05009.0349ecst
6. Yu H-W, Wang T-M, Nguyen H-Q et al (2014) Direct growth of a 40 nm InAs thin film on a GaAs/Ge heterostructure by metalorganic chemical vapor deposition. J Vac Sci Technol B 32:050601. doi:10.1116/1.4892519
7. Fang SF, Adomi K, Iyer S et al (1990) Gallium arsenide and other compound semiconductors on silicon. J Appl Phys 68:R31–R58. doi:10.1063/1.346284
8. Holt DB (1984) Polarity reversal and symmetry in semiconducting compounds with the sphalerite and wurtzite structures. J Mater Sci 19:439–446
9. Morizane K (1977) Antiphase domain structures in GaP and GaAs epitaxial layers grown on Si and Ge. J Cryst Growth 38:249–254. doi:10.1016/0022-0248(77)90305-0
10. Posthill JB, Tarn JCL, Das K et al (1988) Observation of antiphase domain boundaries in GaAs on silicon by transmission electron microscopy. Appl Phys Lett 53:1207. doi:10.1063/1.100021
11. Chu SNG, Nakahara S, Pearton SJ et al (1988) Antiphase domains in GaAs grown by metalorganic chemical vapor deposition on silicon-on-insulator. J Appl Phys 64:2981. doi:10.1063/1.341561
12. Georgakilas A, Stoemenos J, Tsagaraki K et al (1993) Generation and annihilation of antiphase domain boundaries in GaAs on Si grown by molecular beam epitaxy. J Mater Res 8:1908–1921
13. Chriqui Y, Largeau L, Patriarche G et al (2004) Direct growth of GaAs-based structures on exactly (001)-oriented Ge/Si virtual substrates: reduction of the structural defect density and observation of electroluminescence at room temperature under CW electrical injection. J Cryst Growth 265:53–59. doi:10.1016/j.jcrysgro.2004.01.038
14. dos Reis R, Ophus C, Jimenez J et al (2013) Direct atomic imaging of antiphase boundaries and orthotwins in orientation-patterned GaAs. Appl Phys Lett 102:081905. doi:10.1063/1.4793651
15. Holt DB (1969) Antiphase boundaries in semiconducting compounds. J Phys Chem Solids 30:1297–1308. doi:10.1016/0022-3697(69)90191-7
16. Kroemer H (1987) Polar-on-nonpolar epitaxy. J Cryst Growth 81:193–204. doi:10.1016/0022-0248(87)90391-5
17. Petroff PM (1986) Nucleation and growth of GaAs on Ge and the structure of antiphase boundaries. J Vac Sci Technol B 4:874–877. doi:10.1116/1.583529
18. Sakamoto T, Hashiguchi G (1986) Si(001)-2 × 1 single-domain structure obtained by high temperature annealing. Jpn J Appl Phys 25:L78. doi:10.1143/JJAP.25.L78
19. Hamers RJ, Tromp RM, Demuth JE (1986) Scanning tunneling microscopy of Si(001). Phys Rev B 34:5343–5357. doi:10.1103/PhysRevB.34.5343
20. Aspnes DE, Ihm J (1986) Biatomic steps on (001) silicon surfaces. Phys Rev Lett 57:3054–3057. doi:10.1103/PhysRevLett.57.3054
21. Grundmann M (1991) Observation of the first-order phase transition from single to double stepped Si (001) in metalorganic chemical vapor deposition of InP on Si. J Vac Sci Technol B Microelectron Nanometer Struct 9:2158. doi:10.1116/1.585757
22. Volz K, Beyer A, Witte W et al (2011) GaP-nucleation on exact Si (0 0 1) substrates for III/V device integration. J Cryst Growth 315:37–47. doi:10.1016/j.jcrysgro.2010.10.036
23. Ueda O, Soga T, Jimbo T, Umeno M (1989) Direct evidence for self-annihilation of antiphase domains in GaAs/Si heterostructures. Appl Phys Lett 55:445–447. doi:10.1063/1.101870
24. Kim TW, Kang TW, Leem JY et al (1992) Initial stage and reconstruction of GaAs/Si heterostructures. J Mater Sci 27:5603–5608
25. Cho N-H, Carter CB (2001) Formation, faceting, and interaction behaviors of antiphase boundaries in GaAs thin films. J Mater Sci 36:4209–4222. doi:10.1023/A:1017981324721
26. Blakeslee AE, Al-Jassim MM, Asher SE (1987) Origin of defects in MOCVD growth of GaP on silicon. MRS Proc 91:105. doi:10.1557/PROC-91-105
27. Blakeslee AE, Al-Jassim MM, Olson JM et al (1988) GaP/Si heteroepitaxial layers with reduced defect density. MRS Proc 116:313. doi:10.1557/PROC-116-313
28. Liliental-Weber Z, Weber ER, Parechanian-Allen L, Washburn J (1988) On the use of convergent-beam electron diffraction for identification of antiphase boundaries in GaAs grown on Si. Ultramicroscopy 26:59–63. doi:10.1016/0304-3991(88)90377-4
29. Liliental-Weber Z (1989) Methods to decrease defect density in GaAs/Si heteroepitaxy. MRS Proc 148:205. doi:10.1557/PROC-148-205
30. Kim HW (2004) Effect of surface carbon and oxygen on the structural quality of silicon homoepitaxial films. J Mater Sci 39:361–363

31. Yang R, Su N, Bonfanti P et al (2010) Advanced in situ pre-Ni silicide (Siconi) cleaning at 65 nm to resolve defects in NiSix modules. J Vac Sci Technol B 28:56–61. doi:10.1116/1.3271334
32. Akiyama M, Kawarada Y, Ueda T et al (1986) Growth of high quality GaAs layers on Si substrates by MOCVD. J Cryst Growth 77:490–497. doi:10.1016/0022-0248(86)90342-8
33. Biegelsen DK, Ponce FA, Smith AJ, Tramontana JC (1987) Initial stages of epitaxial growth of GaAs on (100) silicon. J Appl Phys 61:1856–1859. doi:10.1063/1.338029
34. Schneider CA, Rasband WS, Eliceiri KW (2012) NIH Image to ImageJ: 25 years of image analysis. Nat Methods 9:671–675. doi:10.1038/nmeth.2089
35. Vajargah SH, Woo SY, Ghanad-Tavakoli S et al (2012) Atomic-resolution study of polarity reversal in GaSb grown on Si by scanning transmission electron microscopy. J Appl Phys 112:093101. doi:10.1063/1.4759160
36. Paladugu M, Merckling C, Loo R et al (2012) Site selective integration of III–V materials on Si for nanoscale logic and photonic devices. Cryst Growth Des 12:4696–4702. doi:10.1021/cg300779v
37. Butz R, Lüth H (1998) The surface morphology of Si (100) after carbon deposition. Surf Sci 411:61–69. doi:10.1016/S0039-6028(98)00328-8